European Option Pricing With a Fast Fourier Transform Algorithm for Big Data Analysis

Shuang Xiao, Shi-Hua Ma, Guo Li, and Samar K. Mukhopadhyay

***Abstract*—Several empirical studies show that, under multiple risks, markets exhibit many new properties, such as volatility smile and cluster fueled by the explosion of transaction data. This paper attempts to capture these newly developed features using the valuation of European options as a vehicle. Statistical analysis performed on the data collected from the currency option market clearly shows the coexistence of mean reversion, jumps, volatility smile, and leptokurtosis and fat tail. We characterize the dynamics of the underlying asset in this kind of environment by establishing a coupled stochastic differential equation model with triple characteristics of mean reversion, nonaffine stochastic volatility, and mixed-exponential jumps. Moreover, we propose a characteristic function method to derive the closed-form pricing formula. We also present a fast Fourier transform (FFT) algorithm-based numerical solution method. Finally, extensive numerical experiments are conducted to validate both the modeling methodology and the numerical algorithm. Results demonstrate that the model behaves well in capturing the properties observed in the market, and the FFT numerical algorithm is both accurate and efficient in addressing large amount of data.**

***Index Terms*—Big data analysis, European option pricing, fast Fourier transform (FFT) algorithm, multiple risks, stochastic modeling.**

Nomenclature

P/Q	Real probability and risk neutral measures.
$E^Q[\cdot]$	Expected function under risk neutral measure Q.
T	Delivery time of a European option.
K	Exercise price of a European option.
$C(\cdot)$	European option price function.
t/u	Time variable, $t/u \in [0, T]$.
$S_t/S_u/S_0/S_T$	Underlying asset price at time $t/u/0/T$.
v_t/v_0	Volatility of the underlying asset price at time $t/0$.
κ/κ^*	Mean-reverting intensity of the underlying asset under different probability measures.
θ/θ^*	Equilibrium mean level of the asset against time under different probability measures.
a/a^*	Equilibrium mean level of the volatility process against time under different probability measures.
b/b^*	Mean reversion speed of the volatility process under different probability measures.
σ	Constant volatility coefficient of the volatility process.
ρ	Correlation coefficient for the two Brownian motions.
η	Nonaffine volatility coefficient of the volatility process.
W_t^1/W_t^2	Two correlated Brownian motions with correlation coefficient ρ in real probability space.
W_t^{1*}/W_t^{2*}	Two Brownian motions corresponding to W_t^1/W_t^2 under risk neutral measure.
$\{V_i\}$	Set of nonnegative stochastic variables, representing the percentage of jump amplitude.
J	Stochastic variable representing the jump amplitude, which follows a mixed-exponential distribution.
λ	Jump intensity, $\lambda > 0$.
$p_u/p_i/\eta_i/q_d/q_j/\theta_j$	Relevant parameters defined in a mixed-exponential distribution.
N_t/N_t^*	Poisson processes with jump intensity $\lambda > 0$ defined in real probability and risk neutral measures, respectively.
$X_t/X_u/X_u$	Log underlying asset price at time $t/u/T$.
X_{t-}/X_{u-}	Value of X_t/X_u just before a jump happens at time t/u.
$\phi_{X_T\|\mathcal{F}_t}(\cdot)/\phi_T$	Characteristic function of log underlying asset price.
$F_{k,u}^{-1}(\cdot)$	Inverse Fourier transformation function.

Manuscript received March 30, 2015; revised June 06, 2015 and October 18, 2015; accepted October 23, 2015. Date of publication November 16, 2015; date of current version June 02, 2016. This work was supported in part by the National Natural Science Foundation of China under Grant 71472069, Grant 71372019, and Grant 71102174; in part by the Beijing Higher Education Young Elite Teacher Project under Grant YETP1173; and in part by the Beijing Philosophy and Social Science Foundation of China under Grant 11JGC106. Paper no. TII-15-1348. *(Corresponding author: Guo Li.)*

S. Xiao and S.-H. Ma are with the School of Management, Huazhong University of Science and Technology, Wuhan 430074, China.

G. Li is with the School of Management and Economics, Beijing Institute of Technology, Beijing 100081, China (e-mail: lg4229682@163.com).

S. K. Mukhopadhyay is with the Graduate School of Business, Sungkyunkwan University, Seoul 110-745, Korea.

Color versions of one or more of the figures in this paper are available online at http://ieeexplore.ieee.org.

Digital Object Identifier 10.1109/TII.2015.2500885

α	Modifying factor and $\alpha > 0$.
r	Risk free interest rate.
k	Log exercise price.
$M(\cdot)/W(\cdot)$	Two Whittaker functions.

I. Introduction

OPTION is being increasingly used as a very important contract for hedging and risk aversion in both financial and operational markets. The Shanghai Stock Exchange issued the first option in the Chinese financial market, called the 50ETF option, on February 9, 2015. In the global industrial procurement, the option contract is commonly used to avoid various kinds of risks, such as price, demand, and foreign exchange rate risks. Therefore, valuing the options more accurately and quickly is of great importance, especially in the big data era.

The best-known among all the option pricing theories is the Black–Scholes (BS) formula, which greatly promoted both the application of options in the market and the rapid development of option theories. Until around 1986, the BS pricing model was proven to be able to depict the market very well. However, the applicability of this model was later widely questioned as a series of mishaps occurred in the financial markets. Prominent among them were the Asian financial crisis during the 1990s and the subprime crisis and the subsequent failure of the Lehman Brothers in the early 21st century. In fact, the traditional BS model does not work when the market risks, such as stochastic volatility and jump risks, increase. Another new development is the advent of the big data era where bulk data handling techniques enable the collection and processing of big and high-frequency data. Many empirical studies show that the mass and high-frequency data demonstrate new properties of the option market, such as leptokurtosis and fat tail, volatility smile, asymmetric distribution, and volatility cluster. To explain these phenomena, many researchers have improved the classical BS model with various methods. We include a review of these improved models in Section II.

In this paper, we consider the European option pricing issue as a vehicle of analysis. We propose an adaptable modeling methodology that could better capture the new properties of the underlying asset when multiple risks exist. We also present an effective and efficient option pricing method to provide a useful tool for practice. Specifically, in contrast to the numerous restrictive assumptions traditionally raised to make the models tractable, we propose only three assumptions that are not overrestrictive and do not take away from the usability of the results. Based on these assumptions, we establish a coupled dynamic model for the log underlying asset under risk neutral measure. We are able to obtain both analytical and numerical solutions for the European option pricing problem. This paper has the following four main contributions.

1) Using a series of empirical performance based on statistical analysis, we demonstrate that, under multiple risks, certain kinds of markets like the currency option market show the characteristics of mean reversion, jumps, volatility smile, and leptokurtosis and fat tail simultaneously. This is verified in Section III.
2) Based on the empirical evidences, the classic BS modeling structure and some relevant research literature, we use the methods of stochastic equations and analyses and establish a general European option pricing model under a risk neutral measure. We prove through a series of numerical experiments that our triple-characteristic stochastic model is able to well-describe the new market properties mentioned above, namely mean reversion, jumps, volatility smile, and leptokurtosis and fat tail.
3) With the methods of characteristic function, we derive the approximate analytical solution for the European option by adopting a number of mathematical tools, such as the generalized Feynman–Kac formula, nonlinear perturbation analysis, and solution techniques for the Ricatti equation.
4) Basing on the analytical solution, we develop a fast Fourier transform (FFT) algorithm to obtain a numerical solution method that does well in addressing large amounts of data. Our numerical experiments demonstrate that the FFT algorithm-based numerical solution method is both effective and efficient compared with the performance of traditional difference Monte Carlo (DMC) simulation.

This paper is organized as follows. We review the literature related to our paper in Section II. Section III provides empirical evidences to demonstrate the validity of the model proposed in this paper. In Section IV, we lay out the basic model for the log underlying asset with properties of mean reversion, nonaffine stochastic volatility, and mixed-exponential jumps. In Section V, we introduce our European options pricing model, both analytically and numerically. In Section VI, we show parts of the results from our extensive numerical experiments. Section VII concludes this paper and indicates some future research directions.

II. Survey of Related Literature

There are three main issues related to our paper, namely, background, modeling, and calculation. Our research was conducted based on the market risk analysis under the environment of big data, and our models were established on the basis of the existing option pricing methods. Moreover, the proposed numerical algorithm for model calculation was greatly inspired by previous works. Therefore, we carry on a thorough literature review in the three dimensions: 1) risk analysis; 2) modeling methods; and 3) numerical algorithms.

A. Risk Analysis

There are a variety of risks that widely exist in different systems. Additionally, as the systems develop, many new kinds of risks emerge. Risk analysis, therefore, is a very important research topic. Some works have focused on exploring new methods to effectively identify, assess, and control risks. In [1], Choi explored the risk levels of a two-echelon supply chain system with vendor managed inventory scheme, and concluded that the radio frequency identification devices (RFID) technology could improve the supply chain resulting in smaller risk. Bernardi *et al.* [2] initiated a comprehensive method to assess

the risk of timing failure by evaluating the software design while a novel approach was proposed in [3] for a distributed real-time coordination and effectively controlled the risks of power flow in the electrical transmission system. Especially, option contract is a very common and useful tool among all kinds of risk controlling strategies. In [4], an option contract was designed to cope with the global supply network risks caused by market volatility and supply disruptions. And a real option approach was used in [5] to control the cost uncertainty risk by allowing a firm to decide when to replace the leased product and remanufacture it.

B. Modeling Methods

The traditional BS model was established under many assumptions. Both the expected return of the underlying asset and its volatility were presumed to be constants. Moreover, it was assumed that the curve of the underlying asset price was continuous. However, these assumptions are widely questioned by a series of practical observations and empirical research works. Therefore, many studies have attempted to improve the BS model from different perspectives. Generally, these modeling methods may fall into three categories, i.e., mean reversion models, stochastic volatility models, and jump models. To capture the mean reversion character observed in markets like commodity, a more general binomial approximation methodology was utilized in [6] to model simple homoscedastic mean-reverting stochastic processes as recombining lattices for real option valuation.

Also, "volatility smile" is a well-known phenomenon. To address this problem, many scholars have explored various modeling methods, among which stochastic volatility models are most widely recognized. In [7], Park and Kim investigated a semianalytic pricing method for look back options in a general stochastic volatility framework. Nearly, all the stochastic volatility models are affine. However, some papers recently found that the nonaffine property of the financial time series existing in reality could not be well described. As a result, there have been several publications that focus on pricing options with the models of nonaffine stochastic volatility. For instance, Yuen and Zheng [8] considered pricing of various types of exotic discrete variance swaps, like the gamma swaps and corridor variance swaps, under the 3/2 nonaffine stochastic volatility models.

Moreover, in practice, various kinds of jumps exist widely in the markets due to factors like wars, economic crises, and real-time market trading. Option pricing problems where the dynamic process of the underlying asset follows a jump-diffusion model have been well explored. A generalized jump-diffusion model was proposed in [9] to price European vulnerable options, and a closed-form price solution was derived by Esscher transform. Furthermore, some papers study option pricing with underlying assets simultaneously exhibiting two kinds of the three properties mentioned above. For instance, Mayer *et al.* [10] initiatively modeled electricity spot prices combining mean reversion and stochastic volatility, and concluded that the model fitted the historical data very well.

C. Numerical Algorithms

Adaptable numerical algorithm for option pricing is another branch of literature closely related to our research. Rapid and accurate pricing of the options, especially in the era of big data, is of great importance in practice. Both traditional and modern numerical algorithms have been proposed for option pricing models. There are some approaches in literature to price options with modern algorithms. In [11], a nonparametric modular neural network (MNN) model was constructed to price the S&P-500 European call options. Most studies focus on the traditional algorithms, though. A novel parallel architecture for accelerating quadrature methods and a least-square Monte Carlo simulation algorithm were proposed to price complex multidimensional options and American multiunderlying stock options in [12] and [13], respectively. Also, a new approximate value iteration method, namely near-value iteration, was presented in [14] to solve continuous-state optimal stopping problems under partial observation. Especially, as a very efficient algorithm, FFT was widely applied in various areas, such as [15] and [16] in signal processing as well as [17] in defense and security systems.

Relying on risk analysis methods presented in Section II-A, we analyze various emerging risks in the big data era, and capture some simultaneously exhibited properties in certain market, which inspire and lay a solid basis for the subsequent modeling and calculation research works. The models reviewed in Section II-B improved the classical BS model through capturing one or two of the several data characteristics. Based on the studies above, we combine the triple characteristics of mean reversion, nonaffine stochastic volatility, and mixed-exponential jumps to establish a general stochastic model. To the best of our knowledge, this type of general stochastic model has not been adequately explored before. Our model is able to depict the phenomena of mean reversion, jumps, volatility smile, and leptokurtosis and fat tail, which are simultaneously observed in some markets like the foreign currency option market. This will be detailed in Section III. Moreover, using the FFT algorithm-based method proposed in Section II-C, we obtain an effective and efficient numerical solution for the proposed model.

III. Empirical Evidence

In this section, we conduct some statistical analysis to show the coexistence of mean reversion, jumps, volatility smile, and leptokurtosis and fat tail in data from real life. To do that, we use data from the currency option market collected from the Saxo Trader platform.

A. Mean Reversion and Jump Phenomenon

To present the phenomenon of mean reversion and jumps, we collected the daily mid-quotes of EURGBP and EURUSD foreign exchange rates for the period between January 1, 2001 and May 18, 2015 as shown in Fig. 1, which visually shows significant mean reversion characteristics of both EURGBP and the

Fig. 1. Historical data series for foreign exchange rates of EURGBP and EURUSD from January 1, 2001 to May 18, 2015.

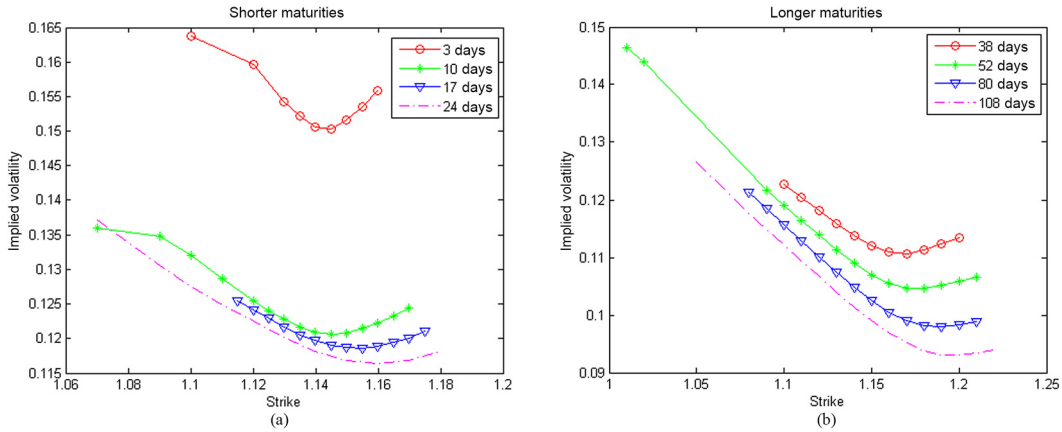

Fig. 2. Market implied volatility smile for different maturities. (a) Shorter maturities. (b) Longer maturities.

EURUSD. Taking the EURUSD as an example, the data show that the Euro had been on a depreciation trend relative to the Dollar from January 1, 2001 through June 2001. Subsequently, the Euro exchange rate increased rapidly until November 2001. In the following 12 years, the Euro exchange rate underwent a number of appreciations and depreciations with respect to the dollar. EURGBP shows similar trends. Additionally, jumps are seen to be obviously occurring frequently in the historical data. We see the exchange rate jumping up, and at other times jumping down. This shows that it is very important to include mean reversion and jumps into option price modeling.

B. Volatility Smile Phenomenon

In order to illustrate the volatility smile phenomenon, we collected data of the observed implied volatilities of the foreign exchange options written on EUR/USD from the trading platform. An example of observed implied volatilities for eight different time-to-maturities on May 18, 2015 is presented in Fig. 2. We observe an obvious volatility smile phenomenon for the currency options, both in short maturities of 3, 10, 17, and 24 days and in long maturities of 38, 52, 80, and 108 days. These empirical evidences strongly suggest that option pricing models should be sufficiently flexible to capture not only the mean reversion and jumps but also the volatility smile.

C. Leptokurtosis and Fat Tail Phenomenon

To figure out whether the leptokurtosis and fat tail phenomenon exists in the currency option market, we conducted statistical analysis on the daily mid-quotes of EURGBP and EURUSD foreign exchange rates from January 1, 2006 through to May 18, 2015. We calculated the daily yields of EURGBP and EURUSD, respectively, and plotted their distributions in Fig. 3. It shows that both the distributions of EURGBP and EURUSD foreign exchange rates are leptokurtosis and have fat tail. More specifically, we calculated that the kurtosis of the two distributions are 9.37 and 7.70, respectively, which are much larger than 3.00, the kurtosis for normal distributions. Thus, it demonstrates that the leptokurtosis and fat tail phenomenon does exist in the currency option market. This analysis motivates us to include the characteristic of leptokurtosis and fat tail when modeling the dynamics of the underlying asset.

IV. Basic Model for Underlying Asset

In this section, we establish a basic stochastic model for the price of an underlying asset. At first, the assumptions are illustrated in detail. Then, the whole procedure for modeling is presented.

As mentioned earlier in Section I, we use the following three assumptions in our modeling.

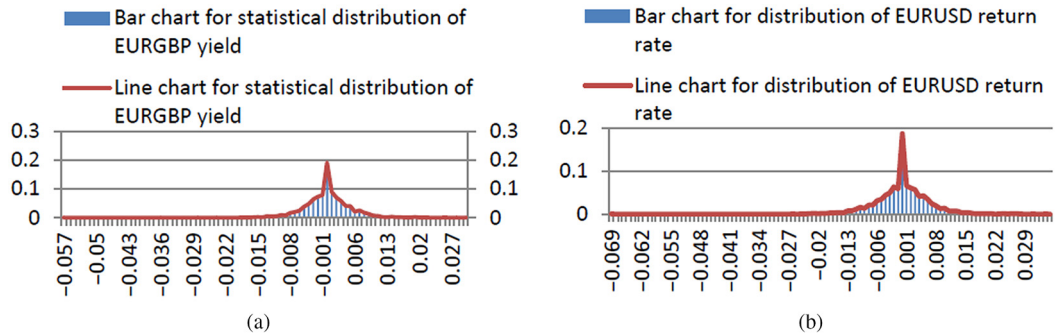

Fig. 3. Statistical distributions for the daily yield of the foreign exchange rate. (a) EURGBP foreign exchange rate. (b) EURUSD foreign exchange rate.

TABLE I
DYNAMIC MODELS FOR OPTION PRICING

Pricing models	Dynamics
Black scholes model (BS)	$dS_t = \mu S_t dt + \sigma S_t dW_t$
Mean reversion model (MS)	$dS_t = \kappa(\theta - \ln S_t)S_t dt + \sigma S_t dW_t$
Stochastic volatility model (SV)	$\begin{cases} dS_t = \mu S_t dt + \sqrt{v_t} S_t dW_{1t} \\ dv_t = \kappa(\theta - v_t)dt + \sigma v_t dW_{2t} \end{cases}$
Normal jump model (NJ)	$\begin{cases} dS_t = \mu S_t dt + \sigma S_t dW_t + JS_t dN_t \\ J \sim \text{Normal}\,(a,b) \end{cases}$

The models are illustrated under objective measures.

Assumption 1: The short-term risk-free interest rate is known and constant through time.

Assumption 2: The market is frictionless, i.e., there are no transaction costs or taxes in the market.

Assumption 3: The market does not pay dividends or other distributions.

Compared to the classical five assumptions normally used for the market of underlying asset, the assumptions proposed here are much weaker, owing to the pricing methods adopted. These three assumptions are used to simplify the model setting and make it more tractable so as to generate meaningful managerial guidelines. Our main results would still hold if these assumptions are relaxed. In case these assumptions are relaxed, the pricing results would surely be more accurate since the basic model would be more consistent with the real-life situation. However, in this paper, we mainly focus on providing a modeling methodology which would better characterize the concurrent properties present in some markets mentioned in the previous sections. The three factors referred in the assumptions are not the key points related to the market properties being considered, so these assumptions do not take away anything from our analysis of the real-life situation.

We now construct the basic log asset price model under the classical BS structure. As detailed in the literature review, many scholars have explored different ways to improve the classic BS model in order to reflect the new features of the market. Several of these main categories are shown in Table I. However, through statistical analysis on empirical data in Section III, we demonstrate that the phenomena of mean reversion, jumps, volatility smile, and leptokurtosis and fat tail do simultaneously occur in some markets. To depict the mean reversion feature, we take the mean reversion item into our model based on the MS model. Also, SV models offer a good approach to address the volatility smile/skew, and according to literature, nonaffine stochastic volatility models have better description effect than the traditional affine one. Therefore, we adopt a nonaffine stochastic process to model the dynamics of the volatility. Moreover, compared to the NJ models, the mixed-exponential distributions can approximate any distribution as closely as possible and thus could simulate various kinds of big and small jumps existing in the market. Hence, we model the jump phenomenon with mixed-exponential jumps.

On the basis of the above analysis, we build a coupled stochastic equation model with triple characteristics of mean reversion, nonaffine stochastic volatility, and mixed-exponential jumps (hereafter referred to as the "triple characteristics model"). The following steps derive our basic model.

A. Basic Triple Characteristic Model

We assume that W_t^1 and W_t^2 are two correlated Brownian motions with correlation coefficient ρ defined in the real probability space $(\Omega, \mathcal{F}, P)$. N_t is a Poisson process with jump intensity coefficient $\lambda > 0$ and is independent from W_t^1 and W_t^2. $\{V_i\}$ is a set of nonnegative stochastic variables which are independent from each other and have identical distributions, representing the percentage of jump amplitude. Let $J = \log(V)$, then J follows a mixed-exponential distribution:

$$J \sim MEJ(p_u, p_i, \eta_i, q_d, q_j, \theta_j),$$
$$i = 1, 2, \ldots, n_1; \quad j = 1, 2, \ldots, n_2$$

with density function

$$g_J(y) = p_u \sum_{i=1}^{n_1} p_i \eta_i e^{-\eta_i y} 1_{\{y \geq 0\}} + q_d \sum_{j=1}^{n_2} q_j \theta_j e^{\theta_j y} 1_{\{y<0\}}$$

in which $p_u \geq 0, q_d \geq 0, p_u + q_d = 1,$ stands for the probabilities that the underlying asset price jumps upward and downward, and

$$p_i \in (-\infty, +\infty), \text{ for } \forall i = 1, \ldots, n_1, \sum_{i=1}^{n_1} p_i = 1$$

$$q_j \in (-\infty, +\infty), \text{ for } \forall j = 1, \ldots, n_2, \sum_{j=1}^{n_2} q_j = 1$$

$$\eta_i > 1, \text{ for } \forall i = 1, \ldots, n_1; \quad \theta_j > 0, \text{ for } \forall j = 1, \ldots, n_2.$$

As p_i and q_j could be negative, these parameters should satisfy certain conditions to guarantee that the density function $g_J(y)$ is both nonnegative and a probability density function. One necessary requirement is: $p_1 > 0, q_1 > 0$, $\sum_{i=1}^{n_1} p_i\eta_i \geq 0$, and $\sum_{j=1}^{n_2} q_j\theta_j \geq 0$. One simple sufficient condition is: $\sum_{i=1}^{k} p_i\eta_i \geq 0$, for $\forall k = 1, \ldots, n_1$, and $\sum_{j=1}^{l} q_j\theta_j \geq 0$, for $\forall l = 1, \ldots, n_2$. To ensure that S_t has a finite expectation, the conditions $\eta_i > 1$ for $\forall i = 1, \ldots, n_1$, and $\theta_j > 0$, for $\forall j = 1, \ldots, n_2$, are necessary. Then the triple characteristics model is

$$\begin{cases} dS_t = \kappa(\theta - \ln S_t)S_t dt + \sqrt{v_t}S_t dW_t^1 + (e^J - 1)S_{t-}dN_t & \text{(1a)} \\ dv_t = b(a - v_t)dt + \sigma {v_t}^{\eta/2} dW_t^2 & \text{(1b)} \\ dW_t^1 dW_t^2 = \rho dt. & \text{(1c)} \end{cases}$$

All parameters have been explained at the beginning of this paper, and especially we select $\eta \in [0, 2]$, representing the nonaffine volatility coefficient of the volatility process.

B. Model Transformation Under Risk Neutral Measure

According to the Girsanov theorem, a risk neutral measure Q exists. In the space under risk neutral measure $(\Omega, \mathcal{F}, Q)$, assume that the risk premium is a linear function of the variance, i.e., $\delta(S_t, v_t, t) = \delta v_t$. Define

$$m = E^Q[V - 1] = p_u \sum_{i=1}^{n_1} \frac{p_i\eta_i}{\eta_i - 1} + q_d \sum_{j=1}^{n_2} \frac{q_j\theta_j}{\theta_j + 1} - 1.$$

Then the models labeled (1a)–(1c) are transformed as below through measure transformation

$$\begin{cases} \frac{dS_t}{S_{t-}} = \kappa^* \left(\theta^* - \ln S_t - \frac{\lambda m}{\kappa^*}\right) dt \\ \qquad\quad + \sqrt{v_t} dW_t^{1*} + (e^J - 1)dN_t^* & \text{(2a)} \\ dv_t = b^*(a^* - v_t)dt + \sigma {v_t}^{\eta/2} dW_t^{2*} & \text{(2b)} \\ dW_t^{1*} dW_t^{2*} = \rho dt & \text{(2c)} \end{cases}$$

where $\kappa^* = \kappa + \delta$, $\theta^* = \frac{\kappa\theta}{\kappa+\delta}$, $b^* = b + \delta$, $a^* = a + \frac{ab}{a+\delta}$, W_t^{1*}, and W_t^{2*} are the standard Brownian motions under risk neutral measure Q with correlation coefficients $\text{corr}(dW_t^{1*}, dW_t^{2*}) = \rho$.

C. Derivation of the Basic Log Asset Price Model

To derive the pricing formula for European options with the underlying asset following dynamics (2a)–(2c) using the characteristic function method, the characteristic function for the log asset price needs to be determined first. Therefore, we define a new stochastic process $\{X_t, t \geq 0\}$ as follows:

$$X_t = \ln S_t. \tag{3}$$

Using the Itô–Doeblin formula, we obtain

$$X_t = X_0 + \int_0^t \frac{1}{S_u} dS_u^c - \frac{1}{2}\int_0^t \frac{1}{S_u^2} dS_u^c dS_u^c + \sum_{0 \leq u \leq t} (X_u - X_{u-}) \tag{4}$$

where S_t^c represents the continuous part of (2a) and X_{t-} means that the value of X_t just before a jump happens at time t. Now, we focus on the jump component for (4). According to the previous descriptions of the jumps, the percentage of the jump amplitude is e^J as long as the jump occurs at time u, i.e., $S_u = e^J S_{u-}$. Hence

$$X_u - X_{u-} = \ln S_u - \ln S_{u-} = J. \tag{5}$$

If the jump does not occur at time u, then $X_u - X_{u-} = 0$. In either case, we have

$$X_u - X_{u-} = J\Delta N_u. \tag{6}$$

According to (6), the jump term can be expressed by

$$\sum_{0 \leq u \leq t} (X_u - X_{u-}) = J \sum_{0 \leq u \leq t} \Delta N_u = \int_0^t J dN_u. \tag{7}$$

Thus, the differential form of (4) is as follows:

$$\begin{aligned} dX_t &= \frac{1}{S_t} dS_t^c - \frac{1}{2}\frac{1}{S_t^2} dS_t^c dS_t^c + J dN_t \\ &= \kappa^* \left(\theta^* - X_t - \frac{\lambda m}{\kappa^*}\right) dt + \sqrt{v_t} dW_t^* - \frac{1}{2} v_t dt + J dN_t. \end{aligned} \tag{8}$$

Based on (2a)–(2c) and (8), we obtain the following stochastic model for the log asset price:

$$\begin{cases} dX_t = \kappa^*(\theta^* - X_t - \frac{v_t}{2\kappa^*} - \frac{\lambda m}{\kappa^*})dt + \sqrt{v_t} dW_t^{1*} + J dN_t^* & \text{(9a)} \\ dv_t = b^*(a^* - v_t)dt + \sigma {v_t}^{\eta/2} dW_t^{2*} & \text{(9b)} \\ dW_t^{1*} dW_t^{2*} = \rho dt. & \text{(9c)} \end{cases}$$

V. Option Pricing: Analytical and Numerical Solutions

In this section, we solve models (9a)–(9c) analytically to obtain the closed-form European option pricing formula with the characteristic function method and its corresponding numerical solution based on the FFT algorithm.

A. Characteristic Function

First, the approximate characteristic function for the log underlying asset X_t is derived based on the following mathematical tools: stochastic analysis, differential equation, and perturbation analysis. The results calculated are illustrated in Theorem 1. The specific derivation details are shown in Appendix.

Theorem 1: We assume that the dynamic process of the log underlying asset $\{X_t, t \in [0, T]\}$ satisfies (9a)–(9c) under risk neutral measure $(\Omega, \mathcal{F}, Q)$ and $X_t = x$, $v_t = v$ at time $t \in [0, T]$. Then, the approximate conditional characteristic function for X_T is of the following form:

$$\phi_{X_T|\mathcal{F}_t}(y) \approx e^{B(t,T) + C(t,T)x + D(t,T)v + iyx} \tag{10}$$

where

$$C(t,T) = iy(e^{-\kappa^*(T-t)} - 1) \tag{11}$$

$D(t,T)$ is derived in (12), which is shown at the bottom of this page.

$$\begin{aligned} B(t,T) = &\left(\frac{\lambda m}{\kappa^*} - \theta^*\right) iy(e^{-\kappa^*(T-t)} - 1) \\ &+ a^* b^* \int_t^T D(x,T)dx \\ &+ \frac{1-\eta}{2} a^{*\eta} \sigma^2 \int_t^T D^2(x,T)dx \\ &+ \frac{\rho\sigma(1-\eta)a^{*\frac{\eta+1}{2}} iy}{2} \\ &\times \int_t^T e^{-\kappa^*(T-x)} D(x,T)dx + \int_t^T \Lambda(x,T)dx \end{aligned} \tag{13}$$

and

$$p = \frac{a^{*\frac{(\eta-1)}{2}}\sigma\eta i - (b^* - \kappa^*)\rho(1+\eta)i}{2\kappa^*\sqrt{4\eta - \rho^2(1+\eta)^2}}, \quad q = -\frac{b^*}{2\kappa^*}$$

$$s = -\frac{\sigma a^{*\frac{(\eta-1)}{2}} y\sqrt{4\eta - \rho^2(1+\eta)^2}}{2\kappa^*}$$

where C_0 is a constant uniquely decided by the boundary value. $M(\cdot,\cdot,\cdot)$ and $W(\cdot,\cdot,\cdot)$ are two Whittaker functions. These functions are two independent solutions to the well-known Whittaker equation and are available in MATLAB software packages.

B. European Option Pricing Formula

Based on Theorem 1, we obtain the European option pricing formula using the method of characteristic function. The result is stated in Theorem 2. Though we use the European call option as an example, this method is also applicable to the European put option.

Theorem 2: We assume that the market of the underlying asset satisfies assumptions 1–3 and the underlying asset price follows the dynamics (1a)–(1c). Then, in the option market, the pricing formula for the European call option with delivery date T and exercise price K is as follows:

$$\begin{aligned} &C(t, X_t, v_t; k, T) \\ &= e^{-r(T-t)-\alpha k} F_{k,u}^{-1}\left[\frac{\phi_{X_T|\mathcal{F}_t}(u-(\alpha+1)i)}{\alpha^2+\alpha-u^2+i(2\alpha+1)u}\right] \end{aligned} \tag{14}$$

where $\phi_{X_T|\mathcal{F}_t}(y)$ is in the forms of (10)–(13) stated in Section V-A, α represents the modifying factor and $\alpha > 0$, $k = \ln K$, and $F_{k,u}^{-1}(\cdot)$ represents the inverse Fourier transformation, as follows:

$$F_{k,u}^{-1}[g(u)] = \frac{1}{2\pi}\int_{-\infty}^{\infty} e^{-iuk} g(u)du.$$

In particular, when $t = 0$, $C(0, X_0; k, T)$ is denoted by $C_T(k)$; $\psi(t, X_t; u, T)$ is denoted by $\psi_T(u)$; and $\phi_{X_T|\mathcal{F}_t}(y)$ is denoted by ϕ_T. We have

$$C_T(k) = e^{-\alpha k} F_{k,u}^{-1}\left[\frac{e^{-rT}\phi_T(u-(\alpha+1)i)}{\alpha^2+\alpha-u^2+i(2\alpha+1)u}\right]. \tag{15}$$

Proof: The conclusions are derived by directly applying the method of characteristic function. ■

C. FFT-Based Numerical Solution

Without loss of generality, let $t = 0$. It is well known that the FFT algorithm could reduce the operand from $O(N^2)$ to $O(N\log_2 N)$, which is a rather considerable reduction in the operation time. FFT is an efficient algorithm to calculate the sum in the following form:

$$w(h) = \sum_{j=1}^{N} e^{-i\frac{2\pi}{N}(j-1)(h-1)} x(j), \quad h = 1, 2, \ldots, N. \tag{16}$$

To adopt the FFT algorithm, transforming (15) into the summation form (16) is necessary. For ease of exposition, let

$$\varphi(u) = \frac{e^{-rT}\phi_T(u-(\alpha+1)i)}{\alpha^2+\alpha-u^2+i(2\alpha+1)u} \tag{17}$$

then (17) is simplified as follows:

$$C_T(k) = e^{-\alpha k} F_{k,u}^{-1}[\varphi(u)] = \frac{e^{-\alpha k}}{2\pi}\int_{-\infty}^{\infty} e^{-iuk}\varphi(u)du. \tag{18}$$

$$\begin{aligned} D(t,T) = &\frac{b^* - \kappa^* - \frac{\rho\sigma(1+\eta)a^{*\frac{\eta-1}{2}} iy}{2} e^{-\kappa^*(T-t)}}{\sigma^2\eta a^{*(\eta-1)}} \\ &+ \frac{2\kappa^*\left(\frac{se^{-\kappa^*(T-t)}}{2} - p\right) M(p,q,se^{-\kappa^*(T-t)})}{\sigma^2\eta a^{*(\eta-1)}[M(p,q,se^{-\kappa^*(T-t)}) + C_0 W(p,q,se^{-\kappa^*(T-t)})]} \\ &+ \frac{2\kappa^*\left(p+q+\frac{1}{2}\right) M(p+1,q,se^{-\kappa^*(T-t)})}{\sigma^2\eta a^{*(\eta-1)}[M(p,q,se^{-\kappa^*(T-t)}) + C_0 W(p,q,se^{-\kappa^*(T-t)})]} \\ &+ \frac{2\kappa^* C_0\left[\left(\left(\frac{se^{-\kappa^*(T-t)}}{2} - p\right) W(p,q,se^{-\kappa^*(T-t)}) - W(p+1,q,se^{-\kappa^*(T-t)})\right)\right]}{\sigma^2\eta a^{*(\eta-1)}[M(p,q,se^{-\kappa^*(T-t)}) + C_0 W(p,q,se^{-\kappa^*(T-t)})]} \end{aligned} \tag{12}$$

TABLE II
PARAMETER SETTING FOR SECTION VI-A

Parameter	κ^*	θ^*	b^*	a^*	σ	ρ	p_u	q_d	n_1	n_2	p_1	q_1	η_1	θ_1	λ	η	S_0	v_0	T
Value	10*	ln1.5	3.33	0.16	0.04	0.9	0.5	0.5	1	1	1	1	2	2	0.11*	1.1*	1.3	0.18	1

*Corresponding values for the parameters are illustrated in the relevant figures when they are variables instead of constants, and we just omit them in the table for ease of presentation.

The trapezoidal rule is applied to the right-hand side of (18), and set

$$u_j = \frac{1-N}{2}\Delta + (j-1)\Delta, \quad j = 1, 2, \ldots, N.$$

Then, the approximate summation form of (18) is

$$C_T(k) \approx \frac{e^{-\alpha k}}{2\pi} \sum_{j=1}^{N} e^{-iu_j k} \varphi(u_j)\Delta. \tag{19}$$

The upper bound of the integral at the right-hand side of (19) is $q^* = N\Delta/2$. Let $k \in [-p^*, p^*]$ and set the step length as l

$$k_h = -p^* + l(h-1), \quad h = 1, 2, \ldots, N \tag{20}$$

then $p^* = Nl/2$.

Substitute (20) into (19), we have

$$C_T(k_h) \approx \frac{e^{-\alpha k_h}}{2\pi} \sum_{j=1}^{N} e^{-i\left(\frac{1-N}{2}\Delta + (j-1)\Delta\right)(-p^* + l(h-1))} \varphi(u_j)\Delta. \tag{21}$$

To transform (21) into the form in (16) so as to adopt the FFT algorithm, it must satisfy

$$l\Delta = 2\pi/N. \tag{22}$$

Equation (22) is substituted into (21) to obtain

$$C_T(k_h) \approx \frac{\Delta e^{-\alpha k_h}}{2\pi} e^{\frac{N-1}{2}\Delta k_h i} \times \sum_{j=1}^{N} e^{-i\frac{2\pi}{N}(j-1)(h-1)} e^{ip^*(j-1)\Delta} \varphi(u_j) \tag{23}$$

where $h = 1, 2, \ldots, N$, and

$$\varphi(u_j) = \frac{e^{-rT}\phi_T(u_j - (\alpha+1)i)}{\alpha^2 + \alpha - u_j{}^2 + i(2\alpha+1)u_j}. \tag{24}$$

Thus far, (15) has been successfully transformed into the form in (16). Next, we could call the FFT algorithm from MATLAB to calculate the price of the European option very quickly.

VI. NUMERICAL EXPERIMENT

In this section, we conduct several numerical experiments to verify both the modeling and solution methodologies proposed in this paper. To validate the proposed model, we need to show whether the model could characterize the simultaneous properties of mean reversion, jumps, volatility smile, and leptokurtosis and fat tail observed in some markets. It is obvious that the basic model theoretically contains characteristics of mean reversion and jumps, thus we only have to conduct analysis on the probability density function and volatility of the underlying asset to see whether the model could reflect the market properties of leptokurtosis and fat tail and volatility smile. We also need to test the validity of the solution methodology. To do that, we compare the effects of the FFT-based numerical solution proposed in this paper with the traditional DMC simulations. All the experiments are implemented on a Pentium Dual 2.0 GHz/2.0 GB personal computer under a Windows XP Professional 2002 version operating system running MATLAB R2012a. For each experiment, the parameters are selected with reference to a previous study [18], and the specific settings are illustrated in each part.

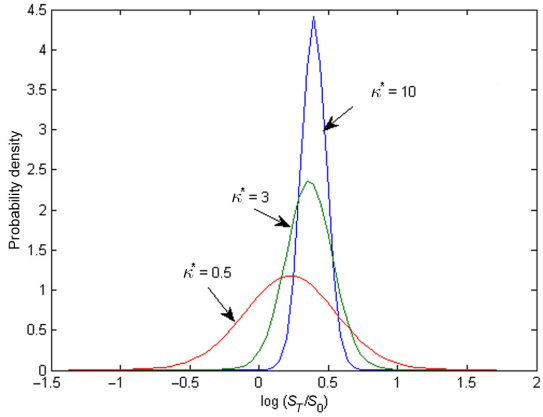

Fig. 4. Probability density function for different values of κ^*.

A. Probability Density Function Analysis

The probability density function of the log underlying asset return can be obtained by inverting Fourier transform on the characteristic function (10). With the capacity of addressing a large amount of data quickly, the FFT algorithm makes it possible to conduct numerical simulations on the probability density function of the log return and examine the properties reflected by the proposed model. All the parameters values are presented in Table II and the impacts of κ^*, λ, b^*, and η on the distribution shape are illustrated in Figs. 4–7. We see that all the distributions show the property of leptokurtosis and fat tail, which is consistent with the characteristics of big data fitting in our empirical study and further validates the effectiveness of our model.

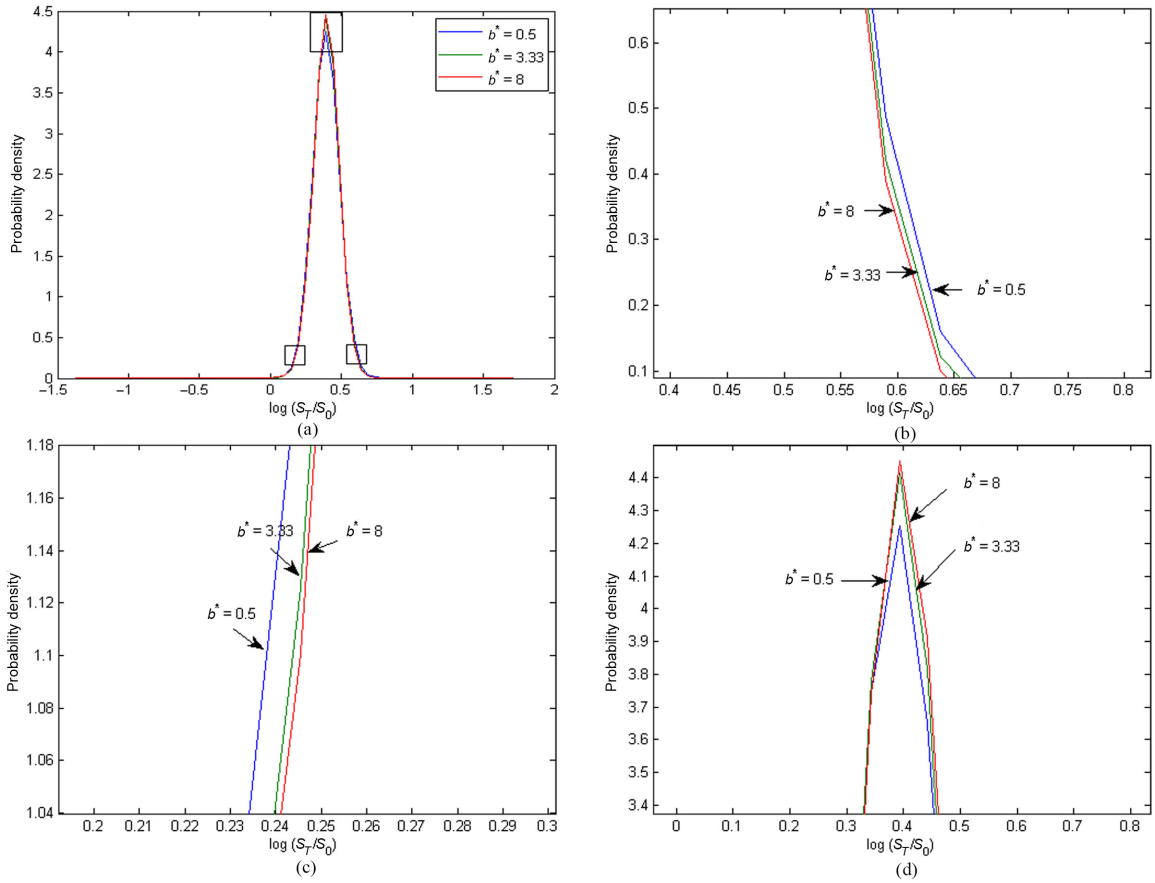

Fig. 5. Probability density functions of the log return of the underlying asset for different values of . (a) Whole figure. (b) Right portion of the whole figure. (c) Left portion of the whole figure. (d) Upper portion of the whole figure.

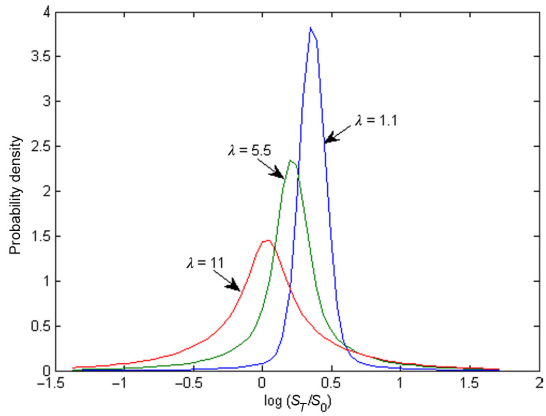

Fig. 6. Probability density functions for different values of λ.

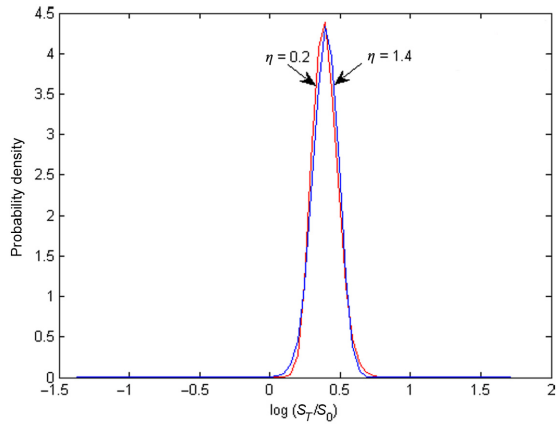

Fig. 7. Probability density functions for different values of η.

Fig. 4 shows how the mean reversion rate of the underlying asset pushes the distribution more toward the equilibrium mean level. When the log return deviates from its equilibrium level, a larger reverting rate helps the log return back to the equilibrium level faster. Consequently, the variance of the distribution is smaller. As shown in Fig. 4, the shape of the distribution is more concentrated when the mean reversion rate of the log return is larger. In real markets, a larger κ^* means a stronger external intervention. For example, in the Chinese market, κ^* may prove to be larger than that obtained in overseas markets because the Chinese government intervenes more in the economy to maintain its stability.

Fig. 5 shows how the mean-reverting rate of the volatility process affects the shape of the distribution. A larger value of b^* means a faster reverting speed for the volatility to its equilibrium level a^*. In our example, the initial volatility value is larger than the equilibrium level. Thus, a quick reverting rate creates a smaller variance of the log return. Moreover, we can observe

TABLE III
PARAMETER SETTING FOR SECTION VI-B

Parameter	b^*	κ^*	σ	ρ	η_1	p_u	r	λ	p_1	n_1	n_2	a^*	θ^*	v_0	S_0	θ_1	q_d	η	T	q_1
Value	3.33	10*	0.04	0.9	2	0.5	0.05	0.11*	1	1	1	0.16	0.40339	0.18	1.3	2	0.5	1.1*	1	1

*Corresponding values for the parameters are illustrated in the relevant figures when they are variables instead of constants, and we just omit them in the table for ease of presentation.

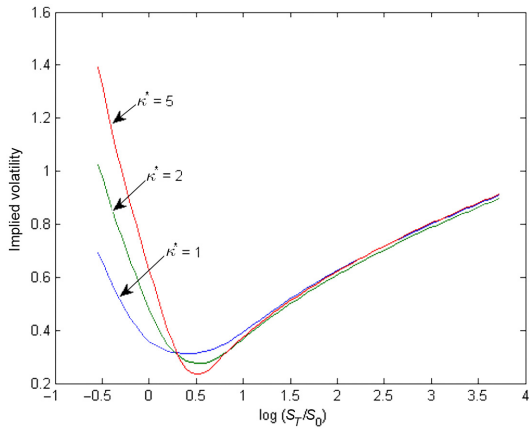

Fig. 8. Implied volatility smile/skew for different values of κ^*.

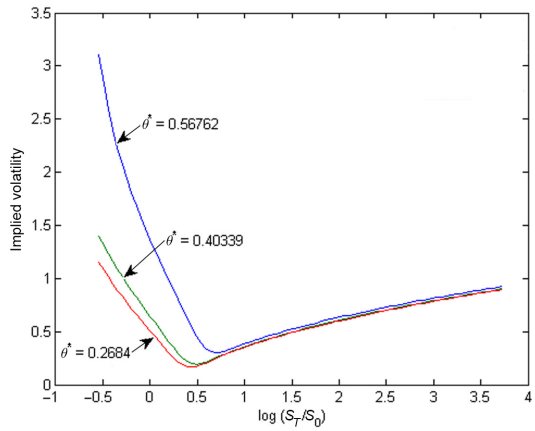

Fig. 9. Implied volatility smile/skew for different values of θ^*.

that a larger b^* makes the distribution more concentrated and have a thinner tail.

The way by which jump intensity λ affects the distribution of the log return is shown in Fig. 6. A larger value of λ means that more jumps can occur at a certain time, causing larger volatility of the underlying asset's log return, resulting in a bigger variance. As seen in Fig. 6, the distribution of the log return is more concentrated with smaller jump intensity λ. For instance, during a financial crisis, the jump intensity can be larger as the disturbance of the financial market increases.

The relationship between the nonaffine volatility coefficient of the volatility process η and the log return of the underlying asset is shown in Fig. 7. It shows that a larger value of η creates a fatter left tail and a thinner right tail of the log return's distribution. When the variance of the log asset is large enough, the volatility's volatility item increases in η, and when the variance is small enough, it decreases in η. Therefore, when the spot asset's price is relatively small, a larger η will make a larger variance of the log return, thereby fattening the left tail of the density function and vice versa.

B. Implied Volatility Smile Analysis

Based on the accurate FFT algorithm, we could further investigate the famous "volatility smile" phenomenon implied by the proposed model. All parameters settings are presented in Table III and the impacts of κ^*, θ^*, λ, and η on the implied volatility are illustrated in Figs. 8–11.

The way by which the implied volatility curve reacts to the different values of κ^* is shown in Fig. 8. The left-tail skew of the volatility smile increases with κ^*, and as κ^* approaches zero, the volatility smile tends to be symmetrical. The relationship between the long-term equilibrium level of the log return of

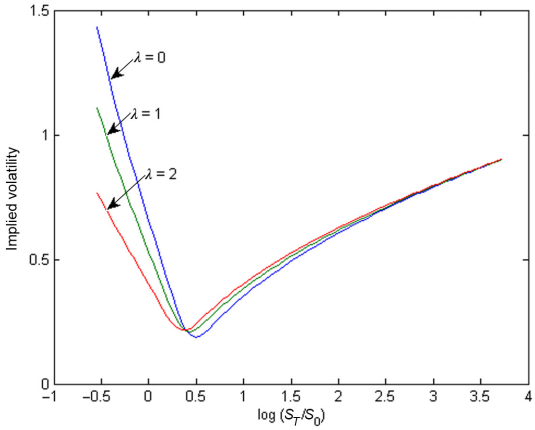

Fig. 10. Implied volatility smile for different values of λ.

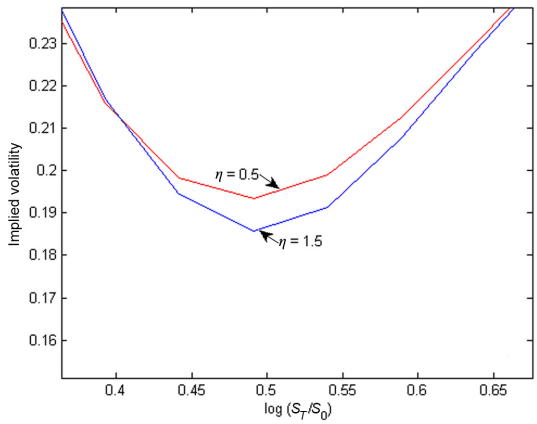

Fig. 11. Probability density functions for different values of η.

TABLE IV
PARAMETER VALUES FOR SECTION VI-C

Parameter	κ^*	θ^*	a^*	b^*	σ	ρ	η	r
Value	10	0.40339	0.16	3.33	0.04	0.9	0.5	0.05
Parameter	S_0	v_0	T	λ	p_u	p_d	n_1	n_2
Value	1.3	0.18	1	0.11	0.5	0.5	1	1
Parameter	p_1	q_1	η_1	θ_1	N	α	Δ	M
Value	1	1	2	2	512	1.5	0.25	50 000

the underlying asset and the volatility smile is shown in Fig. 9. From Fig. 9, we can observe that the left-tail skew increases with the equilibrium value θ^*. A positive correlation coefficient ρ leads to a high variance when the price of the underlying asset rises. Moreover, the price of the underlying asset increases with the equilibrium value θ^*. Therefore, a larger θ^* results in larger variance of the log return, thereby leading to larger implied volatility.

Fig. 10 shows how the jump intensity λ influences the implied volatility smile. We see that when the price of log return is larger than a certain value, the implied volatility increases as the jump intensity decreases. When the price of the log return is smaller than a certain value, the implied volatility decreases, whereas the jump intensity increases.

Fig. 11 shows the effect of the nonaffine volatility coefficient of the volatility process to the implied volatility smile. When the price of the log return of the underlying asset is smaller than some point, a larger nonaffine coefficient η leads to a larger implied volatility. The opposite case is observed when the price of the log return is bigger than that point.

C. Comparison Between FFT and DMC

To verify the efficiency and effectiveness of our proposed method, we use two numerical algorithms to calculate the European call option prices. One is the DMC simulation method based on the dynamic model of the underlying asset price (2a)–(2c) and the other is the FFT algorithm based on the numerical solutions proposed in Section V. Using the results calculated by DMC as a benchmark, we compare FFT with DMC on both accuracy and efficiency. All the parameters used are shown in Table IV.

Using DMC simulation and FFT algorithm to calculate the European option prices with different exercise prices, we obtain the final European option prices in comparison in Table V. A total of 512 evenly-spaced points in the interval $k \in [-4\pi, 4\pi]$, representing 512 different log exercise prices for options with the same underlying asset and delivery time, are selected. As seen in Table V, the European option prices increase with the exercise prices obtained by either FFT or DMC, which is consistent with the option pricing theory. On the other hand, with the option prices computed by DMC as benchmark, the maximum error of results calculated by the FFT is around 0.0708, thus demonstrating that the FFT numerical solution based on the triple-characteristic model is accurate. More importantly, running the FFT algorithm to compute all of the 512 option prices only takes 12.97 min, whereas computing one single option price by DMC when adopting 50 000 paths to approximate the true value takes about 2.47 min. After this comparison, we conclude that when multiple risks exist in the market, the traditional Monte Carlo simulation is no longer a viable method in practice, especially when the data are big. On the contrary, the FFT numerical solution is an efficient tool to address multiple risks and big data.

TABLE V
EUROPEAN CALL PRICES WITH DIFFERENT EXERCISE PRICES: FFT VERSUS DMC

Exercise price	FFT	DMC	Errors
0.821725	0.949253076	0.886697463	0.070548993
0.863068	0.918218627	0.857520099	0.070783795
0.90649	0.886174482	0.842281112	0.052112494
0.952098	0.8530305	0.80792565	0.055827972
1.000000	0.818694917	0.775975186	0.055052961
1.050312	0.783074085	0.740406464	0.057627295
1.103156	0.746072215	0.702606974	0.061862808
1.158658	0.707591128	0.669813408	0.056400364
1.216952	0.667530033	0.632033519	0.056162392
1.342488	0.62578531	0.594622191	0.052408267

VII. CONCLUSION

In the big data era, option pricing becomes more challenging, since it requires more general pricing models that fit the characteristics of big data better and adaptable algorithms to calculate the option prices faster. In this paper, we empirically demonstrate the coexistence of mean reversion, jumps, volatility smile, and leptokurtosis and fat tail in certain markets. To provide a good pricing tool for this kind of market, this paper proposes a modeling methodology as well as both analytical and FFT-based numerical solutions. Through extensive numerical experimentation, the model proposed in this paper is shown to be effective in capturing the multiple features in the market, and the FFT algorithm is also shown to be both accurate and efficient even with big data.

Our work has several limitations. First, to simplify our model, we have used three restricted assumptions. We could, in further research, consider European option pricing problems using empirical methods by extending these assumptions for better pricing accuracy quantitatively besides characterizing the properties of the market qualitatively. Second, in addition to the multiple kinds of objective risks considered in this paper, subjective fuzziness also exists in the market [19]. Therefore, further research can be done to study the option pricing problems in the presence of both randomness and fuzziness.

APPENDIX

Proof of Theorem 1: The characteristic function of X_T satisfying (9a)–(9c) is defined as

$$f(t, x, v; y) = E^Q[e^{iyX_T} | X_t = x, v_t = v]. \tag{A1}$$

According to the generalized Feynman–Kac theorem, $f(y;t,x,v)$ is a solution to the integral partial differential equation integral partial differential equation (IPDE), as follows:

$$\begin{aligned}&\frac{\partial f}{\partial t}+\kappa^*\left(\theta^*-x-\frac{v}{2\kappa^*}-\frac{\lambda m}{\kappa^*}\right)\frac{\partial f}{\partial x}\\&\quad+\frac{1}{2}v\frac{\partial^2 f}{\partial x^2}+b^*(a^*-v)\frac{\partial f}{\partial v}+\frac{1}{2}\sigma^2 v^{\eta}\\&\frac{\partial^2 f}{\partial v^2}+\rho\sigma v^{\frac{\eta+1}{2}}\frac{\partial^2 f}{\partial x\partial v}\\&\quad+\lambda\int_{-\infty}^{+\infty}[f(t,x+z,v;y)-f(t,x,v;y)]g_J(z)dz=0\end{aligned}\tag{A2}$$

with boundary condition

$$f(T,x,v;y)=e^{iyx}\tag{A3}$$

where $g(J)$ is the distribution function of the stochastic variable J.

According to the coefficients of each term in (A2), we know that (A2) is a nonaffine IPDE and the analytical solution cannot be obtained as a rule. Here, we utilize a perturbation method [20] to derive an approximate solution. The main feature of the method relies on approximating v^{η} and $v^{\frac{\eta+1}{2}}$ in the PIDE using Taylor expansion around a^*, which is the long-term mean value of the volatility process, as follows:

$$v^{\eta}=(v-a^*+a^*)^{\eta}\approx(1-\eta)a^{*\eta}+\eta a^{*(\eta-1)}v\tag{A4}$$

$$v^{\frac{\eta+1}{2}}=(v-a^*+a^*)^{\frac{\eta+1}{2}}\approx\frac{1-\eta}{2}a^{*\frac{\eta+1}{2}}+\frac{\eta+1}{2}a^{*\frac{\eta-1}{2}}v.\tag{A5}$$

These approximations result in the following PID:

$$\begin{aligned}&\frac{\partial f}{\partial t}+\kappa^*\left(\theta^*-x-\frac{v}{2\kappa^*}-\frac{\lambda m}{\kappa^*}\right)\frac{\partial f}{\partial x}\\&\quad+\frac{1}{2}v\frac{\partial^2 f}{\partial x^2}+b^*(a^*-v)\frac{\partial f}{\partial v}\\&\quad+\frac{1}{2}\sigma^2\left((1-\eta)a^{*\eta}+\eta a^{*(\eta-1)}v\right)\frac{\partial^2 f}{\partial v^2}\\&\quad+\rho\sigma\left(\frac{1-\eta}{2}a^{*\frac{\eta+1}{2}}+\frac{\eta+1}{2}a^{*\frac{\eta-1}{2}}v\right)\frac{\partial^2 f}{\partial x\partial v}\\&\quad+\lambda\int_{-\infty}^{+\infty}[f(t,x+z,v;y)-f(t,x,v;y)]g_J(z)dz=0.\end{aligned}\tag{A6}$$

As the coefficients of the stochastic differential equations (9a)–(9c) are all linear, according to the theories of linear partial differential equation, the solution to (A6) has the following exponential form:

$$f(t,x,v;y)=e^{B(t,T)+C(t,T)x+D(t,T)v+iyx}\tag{A7}$$

where $B(t,T)$, $C(t,T)$, and $D(t,T)$ are the deterministic functions of t. Through boundary condition (A3), we have

$$B(T,T)=0,\quad C(T,T)=0,\quad D(T,T)=0.\tag{A8}$$

Next, we consider the integral term in (A6)

$$\begin{aligned}&\lambda\int_{-\infty}^{+\infty}[f(t,x+z,v;y)-f(t,x,v;y)]\times g_J(z)dz\\&\quad=f(t,x,v;y)\Lambda(t,T)\end{aligned}\tag{A9}$$

where

$$\begin{aligned}\Lambda(t,T)=\lambda\Bigg(&p_u\sum_{i=1}^{n_1}\frac{p_i\eta_i}{\eta_i-iy-C(t,T)}\\&+q_d\sum_{j=1}^{n_2}\frac{q_j\theta_j}{\theta_j+iy+C(t,T)}-1\Bigg).\end{aligned}$$

The derivation process is based on the fact that the stochastic variable J representing the percentage of jump amplitude is independent from the stochastic process X_t and $J\sim$MEJ$(p_u,p_i,\eta_i,q_d,q_j,\theta_j)$.

By substitution and simplification, we have

$$\begin{aligned}&B_t(t,T)+(\kappa^*\theta^*-\lambda m)(C(t,T)+iy)\\&\quad+a^*b^*D(t,T)+\frac{1-\eta}{2}a^{*\eta}\sigma^2\\&D^2(t,T)+\frac{\rho\sigma(1-\eta)}{2}a^{*\frac{\eta+1}{2}}(C(t,T)+iy)D(t,T)\\&\quad+\Lambda(t,T)=0\end{aligned}\tag{A10}$$

$$C_t(t,T)-\kappa^*(C(t,T)+iy)=0\tag{A11}$$

$$\begin{aligned}&D_t(t,T)+\frac{1}{2}(C(t,T)+iy)(C(t,T)+iy-1)\\&\quad-b^*D(t,T)+\frac{1}{2}\sigma^2\eta\\&\quad\times a^{*(\eta-1)}D^2(t,T)+\frac{\rho\sigma(1+\eta)}{2}\\&\quad\times a^{*\frac{\eta-1}{2}}(C(t,T)+iy)D(t,T)=0\end{aligned}\tag{A12}$$

where $B(t,T)$, $C(t,T)$, and $D(t,T)$ satisfy the boundary conditions in (A8). $B(t,T)$, $C(t,T)$, and $D(t,T)$ are easily solved from (A10)–(A12), and the specific forms are just illustrated in Section V-A.

REFERENCES

[1] T. M. Choi, "Coordination and risk analysis of VMI supply chains with RFID technology," *IEEE Trans. Ind. Informat.*, vol. 7, no. 3, pp. 497–504, Aug. 2011.

[2] S. Bernardi, J. Campos, and J. Merseguer, "Timing-failure risk assessment of UML design using time petri net bound techniques," *IEEE Trans. Ind. Informat.*, vol. 7, no. 1, pp. 90–104, Feb. 2011.

[3] S. C. Muller, U. Hager, and C. Rehtanz, "A multi agent system for adaptive power flow control in electrical transmission systems," *IEEE Trans. Ind. Informat.*, vol. 10, no. 4, pp. 2290–2299, Nov. 2014.

[4] S. Asian and X. Nie, "Coordination in supply chain with uncertain demand and disruption risks: Existence, analysis, and insights," *IEEE Trans. Syst. Man Cybern. Syst.*, vol. 44, no. 9, pp. 1139–1154, Sep. 2014.

[5] W. Shi and K. J. Min, "Product remanufacturing: A real options approach," *IEEE Trans. Eng. Manag.*, vol. 61, no. 2, pp. 237–250, May 2014.

[6] W. J. Hahn and J. S. Dyer, "Discrete time modeling of mean-reverting stochastic processes for real option valuation," *Eur. J. Oper. Res.*, vol. 184, no. 2, pp. 534–548, Jan. 2008.

[7] S. H. Park and J. H. Kim, "A semi-analytic pricing formula for look back options under a general stochastic volatility model," *Stat. Probab. Lett.*, vol. 83, no. 11, pp. 2537–2543, Nov. 2013.
[8] C. H. Yuen and W. Zheng, "Pricing exotic discrete variance swaps under the 3/2-stochastic volatility models," *Appl. Math. Finance*, vol. 22, no. 5, pp. 1–29, Jun. 2015.
[9] F. A. Fard, "Analytical pricing of vulnerable options under a generalized jump–diffusion model," *Insur. Math. Econ.*, vol. 60, pp. 19–28, Jan. 2015.
[10] K. Mayer, T. Schmid, and F. Weber, "Modeling electricity spot prices: Combining mean reversion, spikes, and stochastic volatility," *Eur. J. Finance*, vol. 21, no. 4, pp. 292–315, 2015.
[11] N. Gradojevic, R. Gençay, and D. Kukolj, "Option pricing with modular neural networks," *IEEE Trans. Neural Netw.*, vol. 20, no. 4, pp. 626–637, Apr. 2009.
[12] A. H. Tse, D. Thomas, and W. Luk, "Design exploration of quadrature methods in option pricing," *IEEE Trans. Very Large Scale Integr. Syst.*, vol. 20, no. 5, pp. 818–826, May 2012.
[13] I. Palupi, I. U. Sitorus, and R. F. Umbara, "Using least-square Monte Carlo simulation to price American multi underlying stock options," in *Proc. Int. Conf. Inf. Commun. Technol. (ICoICT'15)*, 2015, pp. 504–509.
[14] E. Zhou, "Optimal stopping under partial observation: Near-value iteration," *IEEE Trans. Autom. Control*, vol. 58, no. 2, pp. 500–506, Feb. 2013.
[15] J. Selva, "FFT interpolation from nonuniform samples lying in a regular grid," *IEEE Trans. Signal Process.*, vol. 63, no. 11, pp. 2826–2834, Jun. 2015.
[16] H. Wen *et al.*, "Harmonic estimation using symmetrical interpolation FFT based on triangular self-convolution window," *IEEE Trans. Ind. Informat.*, vol. 11, no. 1, pp. 16–26, Feb. 2015.
[17] S. McKeown and R. Woods, "Power efficient, FPGA implementations of transform algorithms for radar-based digital receiver applications," *IEEE Trans. Ind. Informat.*, vol. 9, no. 3, pp. 1501–1600, Aug. 2013.
[18] H. Y. Wong and Y. W. Lo, "Option pricing with mean reversion and stochastic volatility," *Eur. J. Oper. Res.*, vol. 197, no. 1, pp. 179–187, Aug. 2009.
[19] V. Behood, J. Lu, and G. Zhang, "Fuzzy refinement domain adaptation for long term prediction in banking ecosystem," *IEEE Trans. Ind. Informat.*, vol. 10, no. 2, pp. 1637–1646, May 2014.
[20] B. Heidergott, H. Leahu, and W. M. Volk-Makarewicz, "A smoothed perturbation analysis of Parisian options," *IEEE Trans. Autom. Control*, vol. 60, no. 2, pp. 469–474, Feb. 2015.

Shuang Xiao was born in Hubei Province, China, in 1988. She received the B.S. degree in mathematics and applied mathematics, and the M.S. degree in operational research and cybernetics from the Huazhong University of Science and Technology, Wuhan, China, in 2011 and 2013, respectively, where she is currently pursuing the Ph.D. degree in management science and engineering at the School of Management.

Her research interests include the financial derivatives pricing, the interface between operation and finance, and supply chain management.

Shi-Hua Ma was born in Tianjin Province, China, in 1956. He received the B.S. degree in machinery manufacturing technology and automation from the Huazhong College of Technology, Wuhan, China, in 1982, and the M.S. and Ph.D. degrees in management science and engineering from the Huazhong University of Science and Technology, Wuhan, in 1990 and 1995, respectively.

He is currently a Professor with the School of Management, Huazhong University of Science and Technology. His research interests include supply chain management, operations management, and logistics management.

Guo Li received the Ph.D. degree in management science and engineering from the Huazhong University of Science and Technology, Wuhan, China, in 2009.

He is an Associate Professor with the School of Management and Economics, Beijing Institute of Technology, Beijing, China. His research interests include supply chain risk management, assembly system, and interface between operation, marketing, and finance. He has authored papers in *Annals of Operations Research,* the *Journal of the Operational Research Society, Transportation Research Part E,* the *International Journal of Production Research*, etc.

Samar K. Mukhopadhyay received the Ph.D. degree in operations management from the University of Texas at Austin, Austin, TX, USA, in 1991.

He is a Professor of Decision Sciences with the Graduate School of Business, Sungkyunkwan University, Seoul, Korea. His research interests include supply chain management and new product development. He has authored papers in *Operations Research,* the *Journal of Operations Management*, *Naval Research Logistics*, *Production and Operations Management*, and other leading journals.

Dr. Mukhopadhyay is a Member of the Editorial Review Board of the *International Journal of Business Analytics*.